Bima Journal of Science and Technology, Vol. 9(2A) Jun, 2025 ISSN: 2536-6041

DOI: 10.64290/bimagombe.v9i2A.1140

Analysis of Optimal Strategy for Effective Control of Cholera Dynamics: A Case Study of Gombe State

Isah Abdullahi[1], Munira Salisu[2], Dauda Gulibur Yakubu[1]*

[1]Department of Mathematical Sciences, Abubakar Tafawa Balewa University, Bauchi, Nigeria
[2]Department of Mathematical Sciences, University of Maiduguri, Borno State, Nigeria

Corresponding Author: dgyakubu@atbu.edu.ng

ABSTRACT

In many regions of sub-Saharan Africa, including Gombe State in Nigeria, cholera is still a major public health concern. In this region (Gombe State), the likelihood and severity of epidemics are increased by factors such as inadequate water sanitation, population displacement, and a lack of adequate healthcare facilities. An extended Susceptible-Infected-Recovered with Contaminated Water (SIR-C) mathematical model that takes into account the three main control strategies of water treatment, vaccine, and curative treatment is developed and examined in this work in response. By incorporating extra treatments specifically designed to address the epidemiological conditions of Gombe State, the model improves an already-existing foundational framework. The transmission dynamics of cholera are simulated using a system of nonlinear differential equations, and important features like disease-free and endemic equilibrium points are investigated analytically, with an emphasis on the local stability as defined by the basic reproduction number (R_0). Numerical simulations are used to support the model, and actual outbreak data from June to December 2022 from the Gombe State Ministry of Health was used to calibrate it. According to comparative simulations, the integrated strategy dramatically lowers the number of infections, flattens the epidemic peak, and shortens the outbreak period, while relying alone on water treatment leads to greater infection peaks and longer epidemic duration. When compared to the single-intervention scenario, the multi-intervention method lowers the infection count by more than 50% at the peak (day 60). These results highlight the critical value of combining vaccination and curative treatment with sanitation efforts. In order to help public health professionals in Gombe State and other susceptible areas to make well-informed decisions regarding cholera management, resource deployment, and outbreak preparedness, the study offers a thorough and context-specific modeling tool that can support public health officials in Gombe State and other vulnerable regions.

Keywords: Cholera, Dynamical system, Optimal control, Transmission, Vaccination

INTRODUCTION

Cholera is a severe and potentially life-threatening acute diarrheal illness that occurs when individuals ingest food or water contaminated with the bacterium *Vibrio cholerae*. This pathogen produces a toxin in the small intestine that triggers massive fluid loss through diarrhea, often leading to dehydration, shock, and, if left untreated, death within hours. The disease spreads rapidly in areas where sanitation is poor and clean drinking water is scarce, conditions common in overcrowded urban slums, refugee camps, and regions experiencing conflict or natural disasters (Zhang *et al.,*2014). This disease has caused seven major pandemics since the 19th century, resulting in millions of deaths worldwide. It remains a significant global health issue, especially in low-and middle-income countries with poor public health infrastructure. Despite being

DOI: 10.64290/bimagombe.v9i2A.1140

preventable and treatable, cholera continues to affect many due to factors such as inadequate water supply, limited healthcare access, and lack of health education (WHO, 2010, 2014).

Cholera is believed to have originated in the Indian subcontinent, particularly around the Ganges River delta, where it had been endemic for centuries. The first recorded pandemic began in 1817, spreading from India to Southeast Asia, America (Andrews & Basu, 2011, Ashliegh et al. 2011, Rasmussen & Mølbak, 2014), the Middle East, and East Africa (Frerichs, 2005). The second pandemic (1829–1837) reached Europe and the Americas, while the third pandemic (1846–1860), the deadliest, furthered cholera's global impact. During this time, British physician John Snow discovered the connection between contaminated water and cholera transmission during an outbreak in London in 1854, laying the foundation for modern epidemiology (Snow, 1855). The current seventh pandemic began in 1961 in Indonesia, driven by the El Tor biotype, and continues to affect regions worldwide, especially areas facing conflict and displacement (WHO, 2018, 2019).

Cholera was first reported in Africa in the 19th century, mainly introduced through European colonial trade routes. The continent faced significant outbreaks during the seventh pandemic, particularly starting in the 1970s (Cappasso & Paveri, 1973), with countries like the Democratic Republic of Congo, Mozambique, and Zimbabwe (Mukandavire et al. 2011and Onuorah et al. 2022) experiencing major epidemics. Africa remains vulnerable to cholera due to poor sanitation, lack of clean water, and weak healthcare infrastructure (Gaffga, Tauxe, & Mintz, 2007). Humanitarian crises, such as those in Somalia, South Sudan, and Ethiopia, have worsened the disease's spread in recent years.

In Nigeria (Figure 1), cholera has been a recurrent health issue since the 1970s, often peaking during the rainy season. Significant outbreaks have occurred in 1991, 2010, and most recently in 2021, with over 100,000 cases and thousands of deaths reported (Nigeria Centre for Disease Control (NCDC, Fatima et al., 2014)). Nigeria's urban slums and internally displaced persons (IDP) camps are particularly vulnerable due to overcrowd living conditions and poor hygiene. Northern Nigeria is especially affected, as factors such as poverty, limited access to clean water, and ongoing security challenges contribute to the spread of cholera. States like Borno, Yobe, and Adamawa face the greatest challenges, with the Boko Haram insurgency displacing millions and creating conditions that facilitate the spread of waterborne diseases. During the 2018 outbreak in Borno State, over 10,000 cases were reported, primarily among displaced populations (UNICEF).

In Gombe State, located in the northeastern region of Nigeria (Figure 1 and 2), cholera has also posed a serious public health threat over the years. Recurrent outbreaks have been documented, often coinciding with the rainy season when water sources become contaminated. Factors such as inadequate access to clean water, poor sanitation infrastructure, and population displacement from neighboring conflict-affected states, and limited healthcare facilities have contributed to the persistence of cholera in Gombe State. Notably, the 2021 national outbreak impacted Gombe State significantly, highlighting systemic vulnerabilities in water management, public health preparedness, and disease surveillance. Previous research has shown that integrated approaches such as combining vaccination campaigns, improved water treatment, and timely medical treatment are far more effective in controlling cholera outbreaks than isolated interventions (Feng et al., 2017).

Bima Journal of Science and Technology, Vol. 9(2A) Jun, 2025 ISSN: 2536-6041

DOI: 10.64290/bimagombe.v9i2A.1140

By incorporating all these elements, a more robust and realistic model can be developed, offering a clearer understanding of how different strategies interact and contribute to cholera control. Such models would be more useful for policymakers and health authorities in Gombe State and other regions, as they would provide evidence-based recommendations for deploying resources and implementing control measures in a way that maximizes their effectiveness. In conclusion, addressing these gaps geographic applicability, context-specific modeling, and the integration of multiple control strategies will be key to developing a more comprehensive and relevant model for cholera control in Gombe State. This will help to ensure that the model can effectively guide interventions, reduce cholera transmission, and ultimately improve public health outcomes in the region.

Given this persistent threat, there is a critical need to enhance existing models of cholera dynamics by incorporating targeted intervention strategies suited to the realities of Gombe State. Previous works by Andam et al. (2015) on Modeling Cholera Dynamics with a Control Strategy in Ghana developed a foundational framework to understand and mitigate cholera spread using water only as the basic control measure. However, to address the unique challenges faced in Gombe State, it is necessary to adapt and extend their model by considering additional control strategies such as vaccination and curative treatment. These interventions are crucial for a more comprehensive and realistic modeling approach that can inform more effective public health responses, particularly in regions facing complex humanitarian and infrastructural challenges.

Figure 1: Map of Nigerian States.

Figure 2: Map of Gombe State with its Local Government Areas (LGAs).

Bima Journal of Science and Technology, Vol. 9(2A) Jun, 2025 ISSN: 2536-6041

DOI: 10.64290/bimagombe.v9i2A.1140

Mathematical Model of SIR-C

In this section, we extend the SIR epidemiological model developed by Andam *et al.* (2015), incorporating water treatment, vaccination, and curative treatment as control strategies, while assuming unequal human birth and death rates. Water treatment is considered a primary control measure due to its crucial role in mitigating cholera outbreaks, with vaccination and curative treatment introduced as additional strategies to reduce disease transmission and enhance recovery. Moreover, in the work of Andam *et al.* (2015), we introduce a new compartment to the model representing the concentration of *Vibrio cholerae* in water at a given time, denoted as $C(t)$. The cholera model now combines human population dynamics and environmental factors (SIR–C), with the total population, $N = S + I + R$, assumed to remain constant. This extension will assess the effectiveness of water treatment, vaccination, and curative treatment as control strategies. The model is based on the following assumptions: water sanitation leads to the death of *Vibrio cholerae* in the aquatic environment; water treatment, vaccination, and curative treatment are the primary control strategies considered; other interventions are not included; human birth and death rates occur at different rates; and cholera is a short-duration disease with low mortality. The variables and parameters used in the model are outlined below as follows:

($S(t)$, $I(t)$ $R(t)$) are susceptible, infected and recovered individual at time t and N total population. $C(t)$ is the concentration of Vibrio cholerae in the water supply at time t, while the remaining parameters are defined explicitly in Table 1.

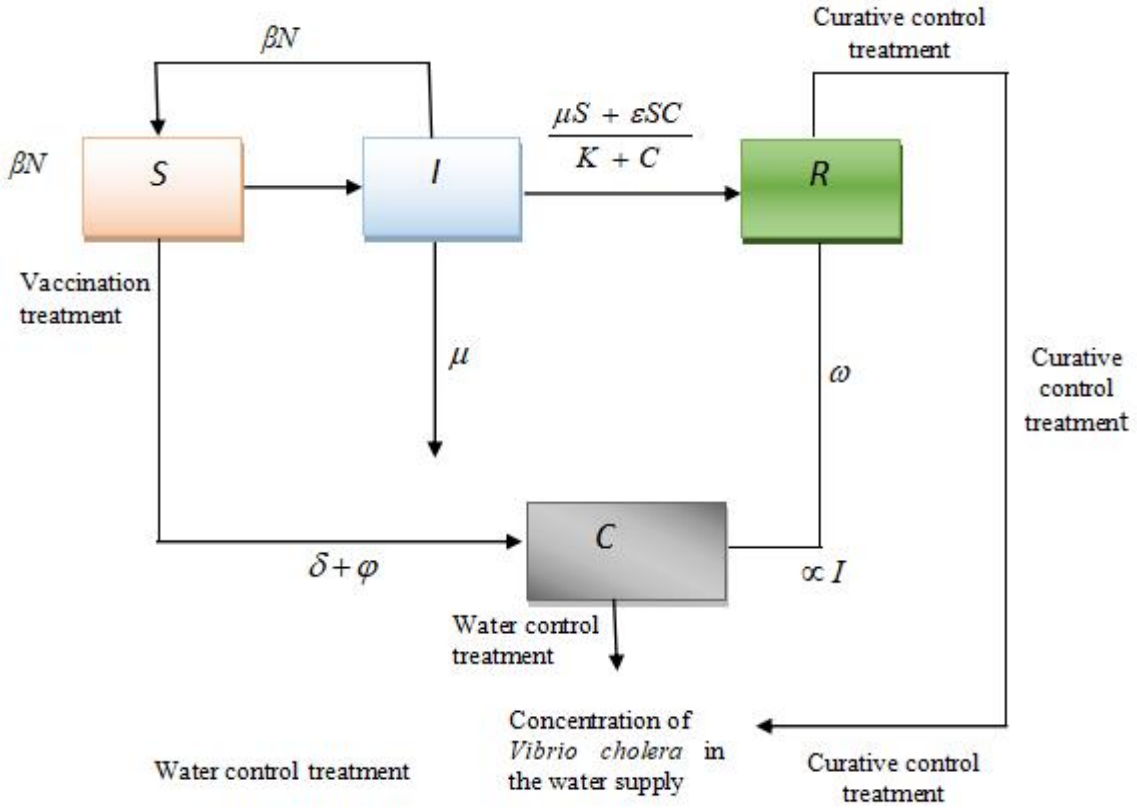

Figure 3: Simplified Schematic Diagram Depicting the Cholera model

DOI: 10.64290/bimagombe.v9i2A.1140

Figure 3 shows the flowchart representing the SIR-C cholera transmission model incorporating three control strategies: vaccination (v), curative treatment (ω), and water sanitation (δ). The model assumes that susceptible individuals (S) are recruited through birth at rate (βN) and become infected (I) upon exposure to contaminated water, with the force of infection governed by

$$-\mu S - vS - \frac{\varepsilon C}{K+C}S.$$

Vaccination reduces the susceptible population, while curative treatment aids recovery. Infected individuals contribute to the environmental concentration of Vibrio cholerae (C) at rate (α), and bacterial loss occurs through natural decay (φ) and water treatment (δ). The total population is considered approximately constant, but human birth and death rates are unequal. Cholera is assumed to have a relatively short infectious period and low mortality.

Based on the assumptions and analysis, the following dynamical systems are derived:

$$\frac{dS}{dt} = \beta N - \mu S - \frac{\xi C}{K+C}S - vS, \quad (1)$$

$$\frac{dI}{dt} = \frac{\varepsilon C}{K+C}S - \gamma I - \mu I - \omega I, \quad (2)$$

$$\frac{dC}{dt} = aI - \delta C - \varphi C, \quad (3)$$

with the conditions

$$S(0) = N(0), I(0) > 0, C(0) > 0. \quad (4)$$

In addition, we have the equation for the R compartment (recovered individuals),

$$\frac{dR}{dt} = \gamma I - \mu R + \alpha(t)I + \upsilon(t)S.$$

Even though this equation is not needed in the model analysis. This is because;

$$R = N - S - I,$$

$$\frac{dR}{dt} = \gamma I - \mu R. \quad (5)$$

SOLUTION OF THE DYNAMICAL SYSTEM

Equation (3) can be reduced to linear form as follows:

$$\frac{dC}{dt} + A_1 C = \alpha I \text{ where, } A_1 = (\delta + \varphi). \quad (6)$$

We also assume at early time *t*,

$$I(t) \approx I_0. \quad (7)$$

Therefore, on substituting equation (7) into equation (6), we have:

$$\frac{dC}{dt} + A_1 C = \alpha I_0, \quad (8)$$

which is now a linear differential equation with integrating factor IF= $\ell^{\int A_1 dt} = \ell^{A_1 t}$.

Multiply equation (8) by the integrating factor (IF) = $e^{A_1 t}$, we have;

$$\frac{d}{dt}(C(t)e^{A_1 t}) = \alpha I_0 e^{A_1 t}. \quad (9)$$

DOI: 10.64290/bimagombe.v9i2A.1140

Integrating equation (9) we have:

$$\int \frac{d}{dt}(CeA_1 t)dt = \alpha I_0 \int e^{A_1 t} dt,$$

$$C(t)e^{A_1 t} = \frac{\alpha I_0}{A_1} e^{A_1 t} t + K_1, \tag{10}$$

where K_1 is the constant of integration, and on simplifying equation (10), we have

$$C(t) = \frac{\alpha I_0}{A_1} + K_1 e^{-A_1 t}. \tag{11}$$

Applying the initial conditions given in equation (4), we have:

$$C_0 = \frac{\alpha I_0}{A_1} + K_1, \text{ which implies that, } K_1 = C_0 - \frac{\alpha I_0}{A_1}. \tag{12}$$

On substituting equation (12) into (11), we obtain the solution of the concentration of *Vibrio cholerae* in the water supply at time *t* as:

$$C(t) = \frac{\alpha I_0}{A_1} + \left[C_0 - \frac{\alpha I_0}{A_1} \right] e^{-A_1 t}. \tag{13}$$

Now, for the solution to the equation (1) and (2), we consider the initial conditions given by:

$$S(t) = N,$$

(Since infection has barely started) and the concentration C, is approximately small. Therefore, we approximate the nonlinear term of equation (1) and (2) as:

$$\frac{C}{K + C} = \frac{C}{K},$$

(since, $C << K$ initially).

Then the approximate form of equation (1) and (2) can be written as:

$$\frac{dS}{dt} = \beta N - \mu S - \frac{\xi CN}{K} - vS, \tag{14}$$

$$\frac{dI}{dt} = \frac{\xi CN}{K} - (\gamma + \varphi)I - \omega I. \tag{15}$$

Now on substituting equation (13) and (15), into (2) we have:

$$\frac{dI}{dt} + (\gamma + \mu)I = \frac{\xi N}{K} \left[\frac{\alpha I}{A_1} + \left[C_0 - \frac{\alpha I_0}{A_1} \right] e^{-A_1 t} \right], \tag{16}$$

$$\frac{dI}{dt} + A_2 I = A_3 + A_4 e^{-A_1 t}, \tag{17}$$

where $A_2 = (\gamma + \mu + \omega)$, $A_3 = \frac{\xi N \alpha I_0}{K A_1}$, $A_4 = \frac{\xi N}{K} \left[C_0 - \frac{\alpha I_0}{A_1} \right]$.

Equation (17) is linear in I(t), therefore using the $IF = e^{\int A_2 dt} = e^{A_2 t}$.

Multiply equation (17) through by $e^{A_2 t}$ we have,

$$\frac{d}{dt}(I(t)e^{A_2 t}) = \left[A_3 + A_4 e^{-A_1 t} \right] e^{A_2 t},$$

DOI: 10.64290/bimagombe.v9i2A.1140

$$\int \frac{d}{dt}(I(t)e^{A_2 t})dt = \int \left[A_3 + A_4 e^{-A_1 t}\right] e^{A_2 t} dt,$$

$$I(t) = \frac{A_3}{A_2} + \frac{A_4}{(A_2 - A_1)} e^{(A_2 - A_1 + A_2)t} + K_2 \ell^{-A_2 t}, \text{where } K_2 \text{ is a constant.} \quad (18)$$

Applying the initial condition in equation (4), yields:

$$I_0 = \frac{A_3}{A_2} + \frac{A_4}{A_2 - A_1} + K_2 \text{ implies that } K_2 = I_0 - \frac{A_3}{A_2} + \frac{A_4}{(A_2 - A_1)}. \quad (19)$$

Putting K_2 into (18) we obtain the number of infected individuals at time *t* as follows:

$$I(t) = \frac{A_3}{A_2} + \frac{A_4}{A_2 - A_1} e^{-A_1 t} + I_0 e^{-A_2 t} - \frac{A_3}{A_2} e^{-A_2 t} - \frac{A_4}{(A_2 - A_1)} e^{-A_2 t}. \quad (20)$$

To obtain the number of susceptible individuals at time t, we put equation (13) into (14) to have,

$$\frac{dS}{dt} + (\mu + v)S = \beta N - \frac{\xi N}{K}\left[\frac{\alpha I_0}{A_1} + \left(C_0 - \frac{\alpha I_0}{A_1}\right)\right] e^{-A_1 t}, \quad (21)$$

$$\frac{dS}{dt} + (\mu + v)S = A_5 + A_6 e^{-A_1 t}, \quad (22)$$

where $A_5 = \beta N - \frac{\xi N}{K A_1}\alpha I_0, \quad A_6 = -\frac{\xi N}{K}\left(C_0 - \frac{\alpha I_0}{A_1}\right)$.

Equation (22) is linear in S(t), hence we use the integrating factor

$$\text{IF} = e^{\int (\mu + \upsilon)dt} = e^{(\mu + \upsilon)t}. \quad (23)$$

Multiply equation (22) by equation (21), we have

$$\frac{d}{dt}\left(S(t)e^{(\mu+\upsilon)t}\right) = \left[A_5 + A_6 e^{-A_1 t}\right] e^{(\mu+\upsilon)t},$$

$$\int \frac{d}{dt}\left(S(t)e^{(\mu+v)t}\right)dt = \left[A_5 + A_6 e^{-A_1 t}\right] e^{(\mu+v)t} dt,$$

$$S(t)e^{(\mu+v)t} = A_5 \int e^{(\mu+v)t} dt + A_6 \int e^{(\mu+v-A_1)t} dt + K_3. \quad (24)$$

On simplifying equation (24), we have

$$S(t) = \frac{A_5}{\mu + v} + \frac{A_6}{(\mu + v - A_1)} e^{(\mu+v-A_1)t} + K_3 e^{-(\mu+v)t}. \quad (25)$$

Applying the initial condition $S(0) = N$, we have:

$$N = \frac{A_5}{\mu + v} + \frac{A_6}{(\mu + v - A_1)} + K_3, \text{ where } K_3 = N - \frac{A_5}{\mu + v} - \frac{A_6}{(\mu + v - A_1)}. \quad (26)$$

On substituting K_3 into (25), we obtain:

$$S(t) = \frac{A_5}{\mu + v} + \frac{A_6}{(\mu + v - A_1)} e^{-A_1 t} + Ne^{-(\mu+v)t} - \frac{A_5}{\mu + v} e^{-(\mu+v)t} - \frac{A_6}{(\mu + v - A_1)} e^{-(\mu+v)t} \quad (27)$$

where the values of $A_1, A_2, A_3, \ldots, A_6$ are explicitly defined in their first appearance.

DOI: 10.64290/bimagombe.v9i2A.1140

Stability Analysis of the Positive Equilibrium Points of the Model

We consider the steady state of the model in equations (1-3) where the solution of particular interest will have non-negative populations ($S(t)$, $I(t)$, $C(t)$) which shows that the system (1-3) has equilibrium points of the form $S(t) \geq 0$, $I(t) \geq 0$, $C(t) \geq 0$. We also assume that the parameters in Table 1 are non-negative. Regarding the vector field and the steady state of the model in equations (1-3), we can easily obtain the equilibrium points by the usual examination of the nullclines, that is, the curves along $S(t) = 0$, $I(t) = 0$, and $C(t) = 0$.

We study the model based on the biological knowledge where the system is regarded to be in the region

$$\Omega = \left\{ \left(S(t), I(t), C(t) \right) \in \Re_+^3 \right\}$$

Here, we present a comprehensive analysis of the stability characteristics associated with the equilibrium points of the proposed model. A thorough analytical investigation was conducted to examine the behavior of the system near these critical points. To assess the stability of the model, we analyzed the system of ordinary differential equations (1–3) that govern the dynamics of the model in a similar fashion as in (Cheng, et al. 2012; Eustace et al. 2018; Jin & Tien, 2011).

The analysis focuses on identifying and examining two biologically meaningful non-negative equilibrium points. The first is the disease-free equilibrium (DFE), which represents a scenario where the infection has been eradicated from the population; mathematically, this corresponds to the condition where the number of infected individuals is zero, that is, $I = 0$. The second is the endemic equilibrium (EE), which characterizes a steady state in which the disease persists within the population at a constant level, implying that $I \neq 0$.

The local and/or global stability of each equilibrium point is determined using suitable mathematical tools such as the Jacobian matrix, eigenvalue analysis, and relevant stability theorems as done in (see, Mohammad & Salisu 2012; Nkuba & Stephen 2015; and Nyaberi & Malonza 2019). This helps to understand under what conditions the disease will die out or persist in the population over time.

Theorem 1.1: *Equations (1-3) show that the endemic equilibrium point of the dynamical system is globally asymptotically stable if* $R_0 < 1$*, and unstable otherwise.*

Existence and stability of the endemic equilibrium

Theorem 1.2: *If every eigenvalue of the Jacobian matrix evaluated at the equilibrium point has a negative real part, then the equilibrium point of the differential equations in (1-3) is stable. If at least one of the eigenvalues has a positive real part, the equilibrium point is unstable.*

Proof.

In order to study the asymptotic behavior of the model in equations (1-3), we find the Jacobian matrix of the model, then substitute the equilibrium point or fixed point obtained into the Jacobian matrix and determine their eigenvalues as shown below. To complete the proof we see that, at the equilibrium point we have,

DOI: 10.64290/bimagombe.v9i2A.1140

$$\frac{dS}{dt} = \frac{dI}{dt} = \frac{dC}{dt} = 0. \quad (28)$$

We therefore equate equations (1)-(3) to zero (0), that is,

$$\beta N - \mu S - \frac{\xi CS}{K + C} - \nu S = 0, \quad (29)$$

$$\frac{\xi C}{K + C} S - \gamma I - \mu I - \omega I = 0, \quad (30)$$

$$\alpha I - \delta C - \varphi C = 0. \quad (31)$$

At the disease-free equilibrium (DFE), there are no infections present in the population; therefore, the infected population, $I = 0$. Substituting this condition into Equation (31), we simplify the system under the assumption of a disease-free state. This substitution allows us to analyze the dynamics of the remaining compartments and facilitates the determination of the stability of the disease-free equilibrium,

$$0 - \delta C - \varphi C = -(\delta - \varphi)C = 0, \quad (32)$$

$$\Rightarrow C = 0, \text{ given that, } \delta - \varphi \neq 0.$$

Putting C=0 into equation (29) we obtain

$$S = \frac{N\beta}{\mu + \nu}. \quad (33)$$

Hence, there exists a disease-free equilibrium (DFE) point, denoted by:

$$(S_0, I_0, C_0) = \left(\frac{N\beta}{\mu + \nu}, 0, 0 \right) = \xi_0, \text{ where } I_0=0, C_0= 0. \quad (34)$$

These values represent the population distribution in the absence of disease, and they are critical for analyzing the local stability of the DFE using techniques such as the Jacobian matrix and the basic reproduction number R_0 .

To investigate the stability of the disease-free equilibrium, we proceed by linearizing the system of the differential equations (1)–(3) around the disease-free equilibrium point. This approach allows us to examine the behavior of small perturbations near the equilibrium state. Specifically, we compute the Jacobian matrix of the system evaluated at the disease-free equilibrium. The Jacobian captures the local dynamics of the system by representing the partial derivatives of each equation with respect to the system's variables. By analyzing the eigenvalues of this Jacobian matrix at the disease-free equilibrium, we can determine the nature of the equilibrium point. If all eigenvalues have negative real parts, the disease-free equilibrium is locally asymptotically stable, meaning that any small deviation from this equilibrium will decay over time and the system will return to the disease-free state. Conversely, if any eigenvalue has a positive real part, the equilibrium is unstable and the disease may invade the population. The Jacobian matrix of the system in equations (1)-(3) is given by:

$$J(S, I, C) = \frac{\partial(f_1, f_2, f_3)}{\partial(S, I, C)}, \quad (35)$$

where

DOI: 10.64290/bimagombe.v9i2A.1140

$$f_1 = \beta N - \mu S - \frac{\varepsilon C}{K+C} S - \nu S,$$
$$f_2 = \frac{\varepsilon C}{K+C} S - \gamma I - \mu I - \omega I, \tag{36}$$
$$f_3 = \alpha I - \delta C - \varphi C.$$

We compute the partial derivatives of f_1, f_2, f_3 respectively as follows:

$$\frac{\partial f_1}{\partial S} = -\mu - \nu - \frac{\xi C}{K+C},$$
$$\frac{\partial f_1}{\partial I} = 0, \tag{37}$$
$$\frac{\partial f_1}{\partial C} = -\frac{\xi S}{K+C} + \frac{\xi CS}{(K+C)^2}.$$

$$\frac{\partial f_2}{\partial S} = \frac{\xi C}{K+C},$$
$$\frac{\partial f_2}{\partial I} = -\gamma - \mu - \omega, \tag{38}$$
$$\frac{\partial f_2}{\partial C} = \frac{\xi S}{K+C} + \frac{\xi CS}{(K+C)^2}.$$

$$\frac{\partial f_3}{\partial S} = 0,$$
$$\frac{\partial f_3}{\partial I} = \alpha, \tag{39}$$
$$\frac{\partial f_3}{\partial C} = -\delta - \varphi.$$

On substituting equations (37)-(39) into the Jacobian matrix, we have;

$$J(S,I,C) = \begin{bmatrix} -\mu - \frac{\xi C}{K+C} - \nu & 0 & -\frac{\xi S}{K+C} + \frac{\xi CS}{(K+C)^2} \\ \frac{\xi C}{K+C} & -\gamma - \mu - \omega & \frac{\xi S}{K+C} + \frac{\xi CS}{(K+C)^2} \\ 0 & \alpha & -\delta - \varphi \end{bmatrix}. \tag{40}$$

Therefore, we evaluate the Jacobian matrix at the equilibrium point;

$$(S_0, I_0, C_0) = \left(\frac{\beta N}{\mu}, 0, 0\right), \tag{41}$$

and hence we get

DOI: 10.64290/bimagombe.v9i2A.1140

$$J(S_0, I_0, C_0) = \begin{bmatrix} -\mu - \nu & 0 & -\frac{\xi\beta N}{\mu C} \\ 0 & -\gamma - \mu - \omega & \frac{\xi\beta N}{\mu C} \\ 0 & \alpha & -\delta - \varphi \end{bmatrix}. \quad (42)$$

The characteristic equation of the Jacobian matrix (42) is given as follows:

$$\det(J(S_0, I_0, C_0) - \lambda I), \quad (43)$$

where I is the identity matrix of appropriate dimension and λ is the roots of the characteristic equation, and hence equation (43) becomes:

$$\left|J(S_0, I_0, C_0) - \lambda I\right| = \begin{vmatrix} -\mu - \nu & 0 & -\frac{\xi\beta N}{\mu C} \\ 0 & -\gamma - \mu - \omega & \frac{\xi\beta N}{\mu C} \\ 0 & \alpha & -\delta - \varphi \end{vmatrix}, \quad (44)$$

which implies that;

$$(-\mu - \nu - \lambda)\left[(-\gamma - \mu - \omega - \lambda)(-\delta - \varphi - \lambda) - \frac{\alpha\xi\beta N}{\mu K}\right] = 0. \quad (45)$$

Therefore, from equation (45), we observe that the characteristic equation of the Jacobian matrix has three roots, and hence;

$$\lambda_1 = -\mu - \nu. \quad (46)$$

Therefore, the remaining two roots will be determine using the quadratic formula

$$\lambda_{2,3} = \frac{-(\delta - \varphi + (\gamma + \mu + \omega)) \pm \sqrt{(\delta - \varphi + (\gamma + \mu + \omega))^2 - 4\left[(\delta - \varphi)(\gamma + \mu + \omega)\frac{\alpha\xi\beta N}{\mu K}\right]}}{2} \quad (47)$$

$$\lambda_{2,3} = \frac{-(\delta - \varphi + (\gamma + \mu + \omega)) \pm \sqrt{(\delta - \varphi + (\gamma + \mu + \omega))^2 - 4[(\delta - \varphi)(\gamma + \mu + \omega)(1 - R_0)]}}{2} \quad (48)$$

$$R_0 = \frac{\alpha\xi\beta N}{\mu K(\delta - \varphi)(\gamma + \mu + \omega)}. \quad (49)$$

According to Andam et al. (2015), R_0 is the basic reproductive number in epidemiology represents the average number of secondary cases generated by a single infectious case over the duration of its infectious period. Now suppose

$$\delta - \varphi < 0, \text{ if } R_0 < 1, \text{ we have, } 4(\delta - \varphi)(\gamma + \mu)(1 - R_0) > 0. \quad (50)$$

Therefore,

$$(\delta - \varphi + (\gamma + \mu + \omega))^2 - 4(\delta - \varphi)(\gamma + \mu + \omega)(1 - R_0) < (\delta - \varphi + (\gamma + \mu + \omega))^2. \quad (51)$$

This implies that

DOI: 10.64290/bimagombe.v9i2A.1140

$$\sqrt{\left(\delta-\varphi+\left(\gamma+\mu+\omega\right)\right)^2-4\left(\delta-\varphi\right)\left(\gamma+\mu+\omega\right)\left(1-R_0\right)}\leq\left(\delta-\varphi+\left(\gamma+\mu+\omega\right)\right). \quad (52)$$

Hence, it can be deduced from equation (48) that;

$$\lambda_{2,3}\leq\frac{-\left(\delta-\varphi+\left(\gamma+\mu+\omega\right)\right)}{2}\pm\frac{\left(\delta-\varphi+\left(\gamma+\mu\right)\right)}{2}, \quad (53)$$

$$\lambda_2\leq\frac{-\left(\delta-\varphi+\left(\gamma+\mu+\omega\right)\right)}{2}+\frac{\left(\delta-\varphi+\left(\gamma+\mu+\omega\right)\right)}{2}, \quad (54)$$

$$\lambda_3\leq\frac{-\left(\delta-\varphi+\left(\gamma+\mu+\omega\right)\right)}{2}-\frac{\left(\delta-\varphi+\left(\gamma+\mu+\omega\right)\right)}{2}. \quad (55)$$

Based on the analysis, it is observed that all the eigenvalues (or roots of the characteristic equation) have negative real parts when the basic reproduction number R_0 is less than 1, that is, $R_0<1$. This indicates that the disease-free equilibrium point is locally asymptotically stable under the condition $R_0<1$, meaning that any small perturbation from the equilibrium will decay over time, and the system will return to the disease-free state. This established the proof of theorem1.2.■

Theorem 1.3: *The dynamical system (1-3) has a disease-free equilibrium point that is locally asymptotically stable if* $R_0<1$*, and unstable otherwise.*

Existence and stability of the endemic equilibrium

The endemic equilibrium of the system of equations (1)–(3) will be determined under the condition where the disease persists in the population. We now proceed to analyze the existence and stability of the endemic equilibrium of the model. To do this, we examine the system at equilibrium, beginning from equation (28), which forms the basis for deriving the steady-state conditions under which the disease remains present in the population, that is,

$$\frac{dS}{dt}=\frac{dI}{dt}=\frac{dC}{dt}=0.$$

We therefore equate equations (1)-(3) to zero (0) to have the following:

$$\beta N-\mu S-\frac{\xi C}{K+C}S-\nu S=0, \quad (56)$$

$$\frac{\xi C}{K+C}S-\gamma I-\mu I-\omega I=0, \quad (57)$$

$$\alpha I-\delta C-\varphi C=0. \quad (58)$$

From equation (58)

$$\alpha I-\delta C-\varphi C=0,$$

$$\alpha I=\left(\delta-\varphi\right)C=0, \quad (59)$$

$$C=\frac{\alpha I}{\delta-\varphi}.$$

Also, from equation (57)

$$\frac{\xi C}{K+C}S-\gamma I-\mu I-\omega I=0,$$

DOI: 10.64290/bimagombe.v9i2A.1140

$$\frac{\xi C}{K+C}S-(\gamma-\mu+\omega)I\,,$$

$$S=\frac{K+C}{\xi C}(\gamma+\mu+\omega)I\,. \tag{60}$$

Again, from equation (56)

$$\beta N-\mu S\frac{\xi C}{K+C}S-\nu S=0\,,$$

$$\beta N-S\left(\mu+\frac{\xi C}{K+C}+\nu\right)=0\,. \tag{61}$$

We then substitute S from equation (60) into equation (61), and simplify as follows:

$$\beta N-\frac{K+C}{\xi C}(\gamma+\mu+\omega)I\left(\mu+\frac{\xi C}{K+C}+\nu\right)=0\,,$$

$$\beta N-(\gamma+\mu+\omega)I\left(\frac{K+C}{\xi C}\mu+\frac{K+C}{\xi C}\times\frac{\xi C}{K+C}+\nu\frac{\xi C}{K+C}\right), \tag{62}$$

$$\beta N-(\gamma+\mu+\omega)I\left(\frac{K+C}{\xi C}(\mu+\nu)+1\right)=0\,. \tag{63}$$

We also substitute C from equation (59) into (63), and simplify as follows:

$$\beta N-(\gamma+\mu+\omega)I\left(\frac{K+\dfrac{\alpha I}{(\delta-\varphi)}C}{\xi\dfrac{\alpha I}{(\delta-\mu)}}(\mu+\nu)+1\right)=0\,,$$

$$\beta N-(\gamma+\mu+\nu)I\left[\left(\frac{K(\delta-\varphi)}{\xi\alpha I}+\frac{1}{\xi}\right)(\mu+\nu)+1\right]=0\,, \tag{64}$$

$$\beta N-\frac{(\gamma+\mu+\omega)IK(\delta-\varphi)(\mu+\nu)}{\xi\alpha I}-\frac{(\gamma+\mu+\omega)I(\mu+\nu)}{\xi}(\gamma+\mu+\omega)I=0\,,$$

$$\beta N-\frac{(\gamma+\mu+\omega)IK(\delta-\varphi)(\mu+\nu)}{\xi\alpha}-(\gamma+\mu+\omega)I\left(\frac{(\mu+\nu)}{\xi}+1\right)=0\,,$$

$$\beta N\xi\alpha-(\gamma+\mu+\omega)K(\delta-\varphi)(\mu+\nu)-(\gamma+\mu+\omega)I\xi\alpha\left(\frac{(\mu+\nu)}{\xi}+1\right)=0\,, \tag{65}$$

$$\beta N\xi\alpha-(\gamma+\mu+\omega)K(\delta-\varphi)(\mu+\nu)-(\gamma+\mu+\omega)I\alpha((\mu+\nu)+\xi)=0\,,$$

$$\frac{\beta N\xi\alpha-(\gamma+\mu+\omega)K(\delta-\varphi)(\mu+\nu)}{(\gamma+\mu+\omega)I\alpha((\mu+\nu)+\xi)}\,. \tag{66}$$

Purportedly, for I >0, we have

$$\beta N\xi\alpha-(\gamma+\mu+\omega)K(\delta-\varphi)(\mu+\nu)\,, \tag{67}$$

DOI: 10.64290/bimagombe.v9i2A.1140

$$\frac{\beta N \xi \alpha}{(\gamma+\mu+\omega)K(\delta-\varphi)(\mu+\nu)} > 1, \quad (68)$$

$$\therefore R_0 > 1,$$

where the Basic Reproductive number, R_0 is given as

$$R_0 = \frac{\beta N \xi \alpha}{(\gamma+\mu+\omega)K(\delta-\varphi)(\mu+\nu)}. \quad (69)$$

The analytical results reveal that a positive endemic equilibrium a steady-state solution where the disease remains present in the population at a constant, non-zero level exists if and only if the basic reproduction number R_0 exceeds 1, that is, when $R_0 > 1$. This threshold condition ($R_0>1$) is both necessary and sufficient for the existence of the endemic equilibrium. In other words, the disease will not persist in the population unless $R_0>1$, and whenever $R_0>1$, a stable endemic state is guaranteed to exist.

Furthermore, this condition holds true regardless of the specific values of the system parameters, provided all parameters remain non-negative, which is consistent with biological and epidemiological realism since parameters such as transmission rates, recovery rates, and natural death rates cannot be negative.

Therefore, it can be concluded that the endemic equilibrium is locally asymptotically stable whenever the basic reproduction number R_0 is greater than one. This means that if the disease is introduced into a population where $R_0>1$, and if the system starts close to the endemic equilibrium, it will naturally evolve back to that equilibrium over time. Thus, the disease will persist and stabilize at a constant level rather than dying out.

NUMERICAL SIMULATIONS AND DISCUSSION OF RESULTS

In this segment to evaluate the effectiveness of various public health interventions, the analytic solutions (see, equations 13, 20, 27) of the model under different control strategies was stimulated, including water treatment alone and a more comprehensive approach combining water treatment, vaccination, and curative treatment. The simulations examine the evolution of key epidemiological variables susceptible individuals, infected individuals, recovered individuals, and pathogen concentration over time. Additional analyses investigate the model's behavior under high-risk transmission conditions, characterized by increased exposure to contaminated water and elevated bacterial contribution from infected individuals. Furthermore, a validation scenario without vaccination or treatment is included to benchmark the model against the original formulation. The results are presented through a series of comparative plots, each highlighting the distinct impact of the control strategies on disease progression, recovery, and environmental contamination. These visualizations provide a foundation for understanding the role of integrated intervention strategies in controlling cholera outbreaks more effectively.

DOI: 10.64290/bimagombe.v9i2A.1140

Table 1: Parameter values used in the cholera model (Hntsa and Kahsay, 2020).

Parameter Symbol	Description	Value	Unit
β (beta)	Birth rate of the population	0.02	per day
μ (mu)	Natural death rate of individuals	0.01	per day
ε (epsilon)	Rate of exposure to contaminated water	0.5 (default), 1.5 (high risk)	per day
γ (gamma)	Recovery rate of infected individuals	0.1	per day
α (alpha)	Contribution of each infected person to the pathogen concentration	0.2 (default), 0.6 (high risk)	unit/pathogen
δ (delta)	Death rate of V. cholerae due to water treatment	0.1	per day
φ (phi)	Natural death rate of V. cholerae in water	0.05	per day
κ (kappa)	Half-saturation constant for exposure	1000000	unit/pathogen
ν (ν rate)	Vaccination rate of susceptible individuals	0.01	per day
τ (tau rate)	Curative treatment rate of infected individuals	0.05	per day
N	Total human population	5612	Individuals
I(0)	Initial number of infected individuals	1000	Individuals
S(0)	Initial number of susceptible individuals	9,000	Individuals
C(0)	Initial pathogen concentration in water	50	unit/pathogen

DOI: 10.64290/bimagombe.v9i2A.1140

Table 2: Time-Based Numerical Validation of Cholera Infection Dynamics Under Single and Multi-Intervention Strategies

S/N	Time (days)	Andam et al. (2015)	Present Study	Difference
1	0	0	0	0
2	10	300	150	150
3	20	800	400	400
4	30	1400	800	600
5	40	2000	1000	1000
6	50	2400	1100	1300
7	60	2600	1250	1350
8	70	2500	1000	1500
9	80	2100	700	1400
10	90	1500	300	1200
11	100	800	100	700

The results presented in the validation Table 2 offer a clear and compelling comparison between the outcomes of the present study and those of Andam et al. (2015) in modeling cholera infection dynamics. It tracks infected population levels over a period of 100 days at 10-day intervals, highlighting the influence of different control strategies on the progression of the epidemic. The model by Andam et al. (2015), which utilizes only water treatment as an intervention, shows a rapid escalation in cases, peaking at approximately 2,600 infected individuals around day 60. In contrast, the present study, which integrates water treatment with vaccination and curative treatment, results in a significantly lower peak of about 1,250 infected individuals at the same time point. Notably, at each interval, the number of infected individuals in the present study is markedly lower than in the Andam et al. (2015) model. For instance, at day 40, the Andam et al. (2015) model records about 2,000 cases compared to only 1,000 in the present study a reduction of 50%. This gap widens further by day 70 and beyond, reflecting the compounded effect of multi-intervention strategies in accelerating outbreak control. Moreover, the present study achieves a quicker decline in infections, reducing the infected population to near-zero by day 100, while the Andam et al. (2015) model still reflects a considerable number of active cases (approximately 800) at that point.

This numerical validation underscores the advantage of incorporating multiple, complementary control strategies in epidemic modeling. The present study demonstrates superior effectiveness in reducing both the magnitude and duration of the outbreak, ultimately confirming that a multi-pronged approach leads to faster containment, lower infection burden, and better public health outcomes. The findings validate the enhanced SIR-C model's applicability in real-world settings like Gombe State and affirm its potential utility as a planning tool for public health interventions.

Bima Journal of Science and Technology, Vol. 9(2A) Jun, 2025 ISSN: 2536-6041

DOI: 10.64290/bimagombe.v9i2A.1140

Table 3: Cholera cases in Gombe state center for infectious disease and leprosy control in Zambuk Covering the 11 local governments from June to December (2022).

Location	June	July	Aug.	Sept.	Oct.	Nov.	Dec.	Total
Akko	208	84	32	26	18	19	33	420
Bajoga/Nafada	194	96	96	14	12	11	22	445
Balanga	203	94	94	15	10	21	20	457
Billiri	232	103	103	17	13	18	18	504
Dukku	235	94	94	10	19	8	21	481
Funakaye	280	78	78	15	23	9	27	510
Gombe	213	97	97	14	15	12	20	468
Kaltungo	233	98	98	21	17	17	27	511
Kwami	220	98	98	19	10	19	28	492
Shongom	214	119	119	16	11	14	20	510
Yamaltu/Deba	290	125	29	0	2	0	17	463

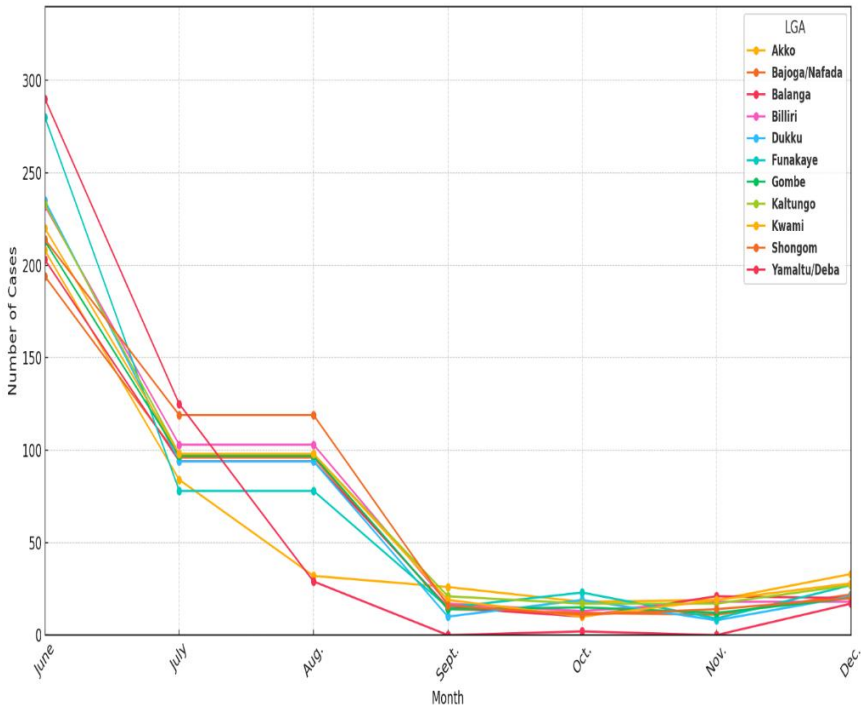

Figure 4: Monthly Distribution of Cholera Cases Across Gombe State LGAs (June–Dece. 2022).

DOI: 10.64290/bimagombe.v9i2A.1140

The line graph in Figure 4 illustrates the monthly distribution of cholera cases across the 11 Local Government Areas (LGAs) of Gombe State from June to December 2022. A clear pattern emerges showing that the outbreak was more severe in June, with nearly all LGAs reporting their highest case numbers during that month. Notably, Yamaltu/Deba recorded the peak incidence with 290 cases, followed closely by Funakaye and Dukku. This widespread spike in June suggests a state-wide outbreak or environmental conditions highly conducive to cholera transmission during that period. Following June, a significant decline in cholera cases is observed across most LGAs. For example, Akko dropped from 208 cases in June to just 32 in August, indicating effective intervention measures or natural containment. While this downward trend was consistent in several areas, some LGAs, such as Billiri, Kaltungo, and Balanga, maintained relatively stable and moderately high case numbers between July and October. These sustained levels suggest localized challenges in controlling the outbreak, possibly due to persistent risk factors or inadequate health infrastructure. By November and December, the graph shows that the outbreak had largely subsided in most LGAs. Yamaltu/Deba, for instance, reported zero cases in September and November, reflecting a temporary halt in transmission. However, Kaltungo and Shongom stand out as exceptions, with both areas continuing to report moderate levels of infection until the end of the year. This persistence indicates potential gaps in containment efforts or environmental conditions that sustained the transmission longer than in other regions.

Therefore, the graph reveals a cholera outbreak that peaked in June and generally declined over the subsequent months, with varying rates of reduction across the LGAs. While many areas successfully reduced cases, a few continued to experience significant transmission, highlighting the need for targeted public health responses in those specific locations.

The alarming surge in cholera cases across the 11 Local Government Areas of Gombe State between June and December 2022, as reflected in the reported data, highlights the urgent need for a systematic and predictive approach to understanding and managing the outbreak. The pattern of infections marked by a severe peak in June followed by irregular declines suggests that various environmental, behavioral, and intervention-related factors are at play.

This is where a mathematical model becomes crucial. Mathematical models provide a structured framework for capturing the transmission dynamics of cholera by incorporating key elements such as the susceptible population, infected individuals, environmental bacterial concentration, recovery rates, and intervention effects. These models help simulate different scenarios and forecast the course of the outbreak under various control strategies. In particular, they allow health authorities to answer critical "what-if" questions for example, what would happen if vaccination coverage were increased, or how quickly a water sanitation campaign could suppress bacterial concentration (Hntsa and Kahsay, 2020).

In light of the persistent and widespread nature of the outbreak in Gombe State, the mathematical model proposed by Andam et al. (2015) becomes especially relevant. The model was originally developed to study cholera transmission dynamics with environmental factors and interventions such as water sanitation and treatment. However, to address the unique socio-environmental and epidemiological context of Gombe State, it was necessary to adapt and extend the Andam et al. (2015)s' model. The extension integrates

DOI: 10.64290/bimagombe.v9i2A.1140

the impact of combined interventions specifically, water vaccination programs and curative treatments which were not explicitly addressed in the original formulation.

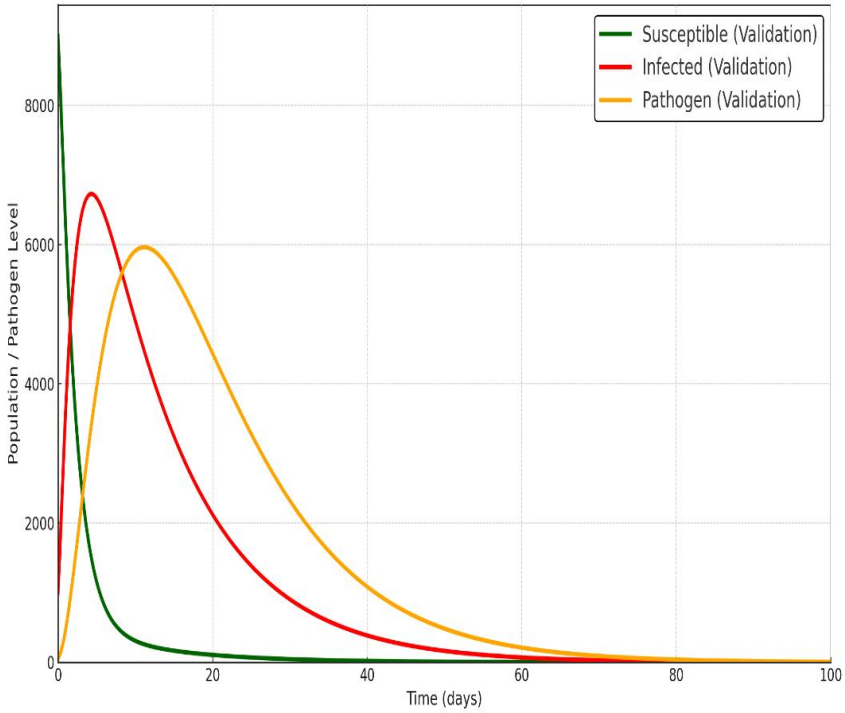

Figure 5: Model Validation: Susceptible, Infected, and Pathogen Trajectories with Zero Additional Controls.

Figure 5 illustrates the validation of the temporal progression of the three core components of the cholera transmission model susceptible individuals, infected individuals and the concentration of *Vibrio cholerae* in the environment. In this simulation, no additional interventions such as vaccination or curative treatment are implemented; instead, the model reflects a baseline scenario in which the only control mechanism is water treatment, and disease progression follows its natural course. This setup is particularly important because it provides a reference point against which the impact of more comprehensive control strategies can be measured. The dynamics shown in the graph demonstrate the inherent limitations of relying solely on water sanitation. The susceptible population gradually decreases as more individuals become infected over time due to ongoing exposure to contaminated water. The infected population rises sharply to a peak, indicating the onset of an outbreak, and only slowly declines thereafter, showing the prolonged impact of infection in the absence of targeted interventions. Meanwhile, the concentration of pathogens in the environment remains elevated for an extended period, reflecting sustained contamination from infected individuals and the slow decay of bacteria despite water treatment efforts. Overall, this graph validates the baseline structure of the model with only water as a control. It serves as a critical benchmark for assessing the effectiveness of additional control strategies in subsequent simulations and highlights the need for integrated public health responses to effectively suppress cholera outbreaks.

Bima Journal of Science and Technology, Vol. 9(2A) Jun, 2025 ISSN: 2536-6041

DOI: 10.64290/bimagombe.v9i2A.1140

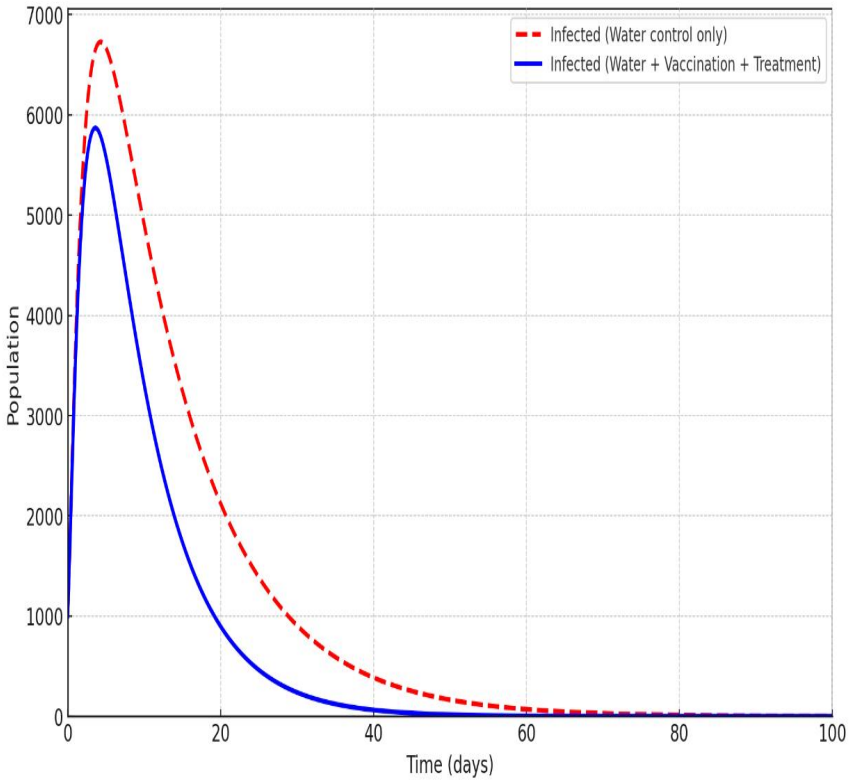

Figure 6: Impact of Water Treatment Alone Versus Combined Control Strategies on Cholera Infections

The plotted graph in Figure 6 illustrates the comparative dynamics of cholera infections under two different control strategies. The red dashed line represents the original model by Andam et al. (2015), where only water treatment is employed as a control measure. In this Figure, the number of infected individual increases rapidly at the onset, indicating a swift spread of the disease following exposure to contaminated water. The peak of infections is relatively high and the decline is gradual, suggesting that while water treatment helps, it is not sufficient to bring the epidemic under control quickly. Infections persist in the population for a longer duration, which implies sustained environmental contamination and ongoing transmission.

In contrast, the blue solid line incorporates additional interventions vaccination and curative treatment alongside water control. This combined approach results in a significantly lower and earlier peak in the number of infected individuals. The decline in infections is more rapid, demonstrating the effectiveness of vaccination in reducing the susceptible population and of treatment in speeding up recovery. Consequently, the outbreak is controlled more efficiently, and the overall number of infections is markedly reduced. This suggests that integrating multiple control strategies has a synergistic effect on curbing the spread of cholera.

Therefore, the results from the Figure indicate that while water treatment plays an essential role in managing cholera, its impact is limited when used in isolation. The addition of vaccination and curative treatment not only lowers the infection burden but also shortens the epidemic duration, highlighting the importance of a comprehensive and coordinated public health response in the control of cholera outbreaks.

Bima Journal of Science and Technology, Vol. 9(2A) Jun, 2025 ISSN: 2536-6041

DOI: 10.64290/bimagombe.v9i2A.1140

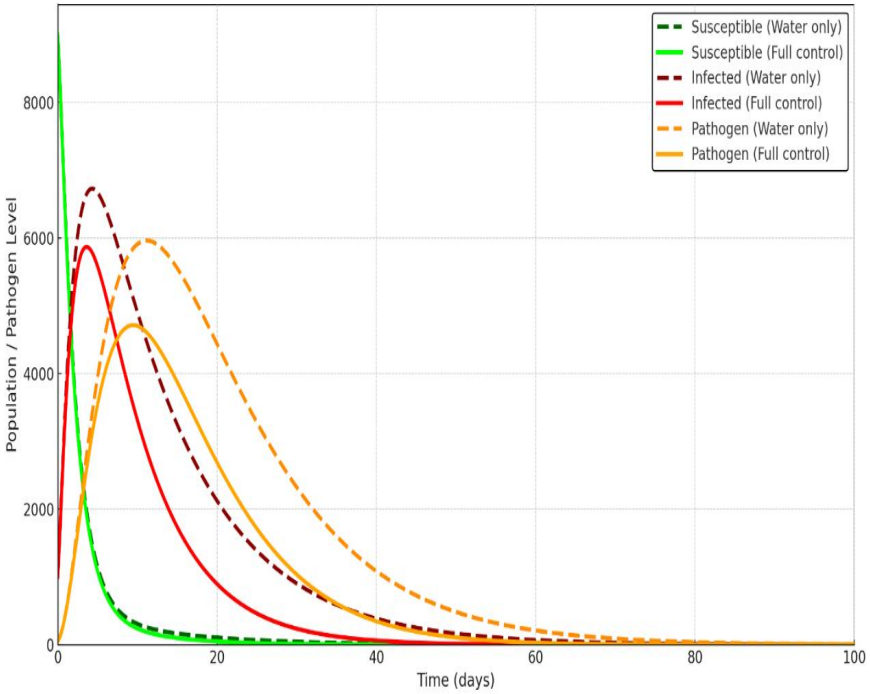

Figure 7: Comparative Analysis of Model Components under Water-Only and Combined Control Strategies

The graph in Figure 7 presents a detailed comparison of cholera dynamics under two scenarios: one with only water treatment, and the other with a comprehensive intervention that includes water treatment, vaccination, and curative treatment. It tracks the trajectories of three key components of the disease model susceptible individuals (S), infected individuals (I), and pathogen concentration in the environment (C) over time.

In the susceptible population curves, the green dashed line (water control only) shows a gradual decline as more individuals become infected over time. In contrast, the bright green solid line (full control) declines more sharply initially due to the additional effect of vaccination, which moves individuals directly out of the susceptible pool without infection. This demonstrates the preventive capacity of vaccination in reducing the at-risk population from the onset, thereby narrowing the window for widespread transmission. The infected population curves show the most striking difference. Under water control only (deep red dashed line), infections surge rapidly to a higher peak and take a long time to decline. This indicates that water treatment alone, while useful, is not sufficient to control the outbreak swiftly. In contrast, the full control scenario (bright red solid line) results in a significantly lower peak and a much faster decline. The combination of vaccination and treatment limits both the number of new infections and the duration of infectiousness, effectively flattening and shortening the epidemic curve. This reflects a more robust and timely suppression of the outbreak. The pathogen concentration in water follows a similar pattern. The orange dashed line (water-only control) remains high for an extended period, implying ongoing contamination due to untreated infected individuals. Meanwhile, the bright orange solid line (full control) shows a quicker and lower peak, with a faster reduction in environmental contamination. This is due to the reduced number of infected

DOI: 10.64290/bimagombe.v9i2A.1140

individuals contributing *Vibrio cholerae* to the water supply and the continued efficacy of water treatment.

Therefore, the results in Figure 7 illustrate the substantial added value of incorporating vaccination and treatment alongside water control. Not only do these interventions protect uninfected individuals and hasten recovery, but they also reduce environmental contamination, which is a major transmission route for cholera, as suggested by Usamani et al. (2021). The full control strategy leads to a shorter outbreak, fewer infections, and a faster return to normalcy, making it a more effective and sustainable approach to epidemic management. These findings highlight the importance of a multi-faceted public health response in addressing waterborne diseases like cholera, particularly in resource-limited settings where outbreaks can escalate quickly without comprehensive control measures.

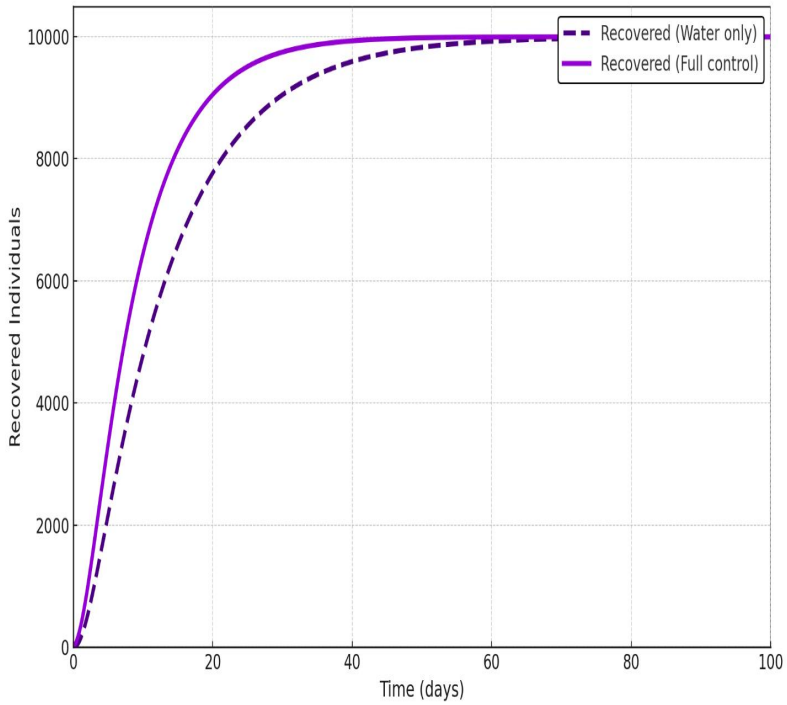

Figure 8: Effect of Control Strategies on Recovered Individuals in the Population

Figure 8, represents the plot of the recovered individuals over time provides important insight into the long-term effectiveness of the control strategies used to manage cholera. It highlights the contrasting recovery outcomes between the scenario using only water treatment and the more comprehensive approach that combines water treatment, vaccination, and curative treatment. In the case of water treatment alone (represented by the dashed purple line), recovery occurs steadily but relatively slowly. Since no vaccination is employed and treatment is limited to environmental sanitation, infected individuals recover at a natural rate, which prolongs the time they remain infectious. This results in a slower accumulation of recovered individuals. The curve rises gradually, and it takes a longer time to reach a plateau, reflecting the persistent presence of the disease in the population. On the other hand, the combined control strategy (solid violet line) leads to a more rapid and pronounced increase in recovered individuals. This is primarily due to

DOI: 10.64290/bimagombe.v9i2A.1140

the inclusion of curative treatment, which shortens the duration of infection and accelerates recovery. Additionally, vaccination reduces the number of individuals who ever become infected, indirectly boosting the relative proportion of the population that transitions to the recovered state through early intervention. As a result, the recovery curve under full control climbs more quickly and reaches a higher plateau in a shorter time span. The overall shape of the recovery curves reveals how quickly a population can achieve partial or full immunity after an outbreak, which is critical in stopping the spread of cholera. A faster increase in recovered individuals contributes to reducing the susceptible population and slows down transmission. In this context, the full control strategy not only prevents new infections but also promotes a swifter restoration of public health by facilitating quicker recovery. Therefore, the graph confirms that while water treatment plays a key role in limiting environmental exposure, the integration of vaccination and treatment is essential for accelerating recovery, limiting the burden of disease, and reducing the overall duration and impact of the epidemic. This supports the case for adopting multi-pronged control measures in real-world cholera prevention and response strategies.

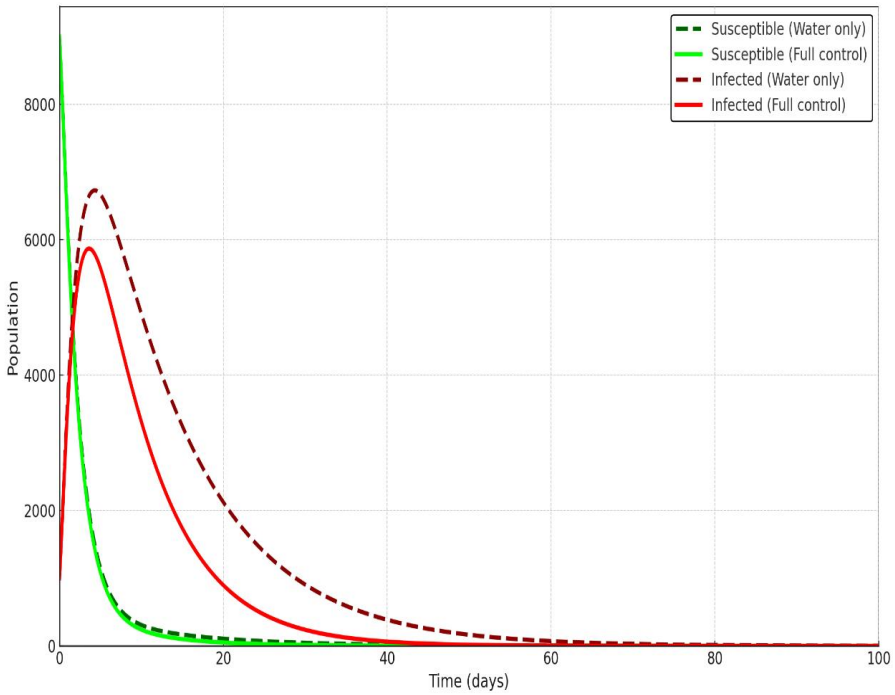

Figure 9: Susceptible and Infected Population Dynamics with and without Control Interventions.

The plot in Figure 9 compares the trajectories of susceptible and infected individuals over time under two different intervention strategies: water treatment only and a combined strategy including water treatment, vaccination, and curative treatment. The purpose of this comparison is to understand how these strategies influence the spread and containment of cholera in the population.

In the case of susceptible individuals, the dashed green line (water-only control) shows a gradual decrease in the susceptible population.

DOI: 10.64290/bimagombe.v9i2A.1140

This decline is due to the fact that susceptible individuals are exposed to the bacteria and become infected over time. Since no vaccination is applied in this scenario, the only way individuals exit the susceptible class is through infection. As a result, the decline is slow and continues for a longer period, leaving a large portion of the population vulnerable for an extended time. On the other hand, the solid green line (full control) shows a steeper and more rapid decline in the susceptible population. This is primarily due to the addition of vaccination, which removes individuals from the susceptible class before they have a chance to be infected. Consequently, the pool of individuals at risk is reduced quickly, which plays a critical role in limiting the spread of the disease. The difference is even more pronounced in the infected population curves. The dashed red line (water-only control) indicates a sharp increase in infections shortly after the introduction of *Vibrio cholerae*, followed by a slow decline. The high peak and prolonged presence of infected individuals reflect the limited effectiveness of water treatment alone in controlling the epidemic, especially when initial exposure is high. In contrast, the solid red line (full control) shows a much lower peak of infection and a significantly faster decline. The rapid drop is a result of curative treatment, which reduces the duration of infection, and vaccination, which prevents many individuals from becoming infected in the first place. This leads to a much shorter outbreak period and reduces the overall burden on the population and healthcare systems. In essences, the plot clearly demonstrates the superior effectiveness of a comprehensive control strategy. While water treatment helps by reducing environmental transmission, it is not enough to control cholera quickly or completely. Adding vaccination and curative treatment significantly reduces the number of susceptible and infected individuals, curtails the spread of the disease, and accelerates the resolution of the outbreak. These findings support the importance of integrated approaches in managing cholera epidemics as also pointed out by Wang and Modnak, (2011).

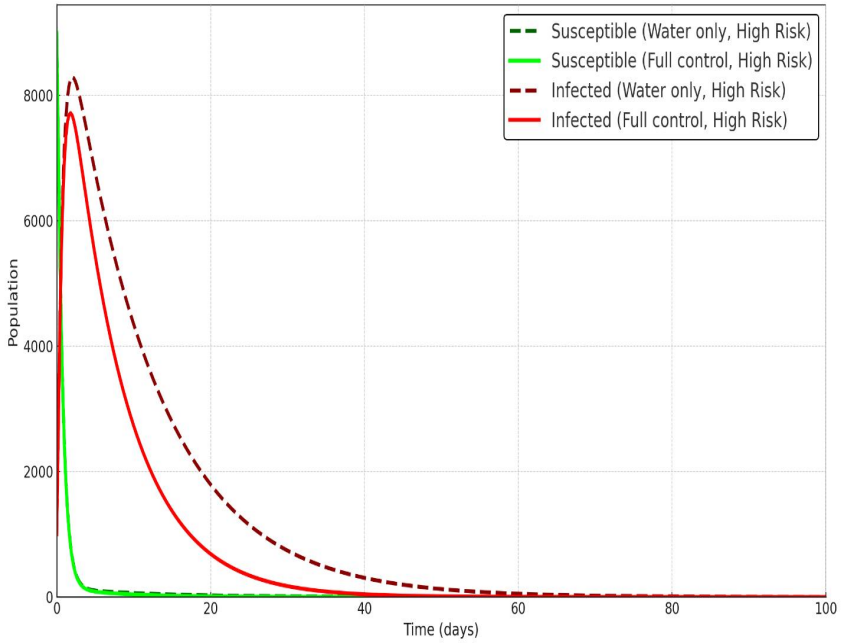

DOI: 10.64290/bimagombe.v9i2A.1140

Figure 10: Susceptible and Infected Population Dynamics under High-Risk Environmental Conditions

Figure 10, illustrates the cholera outbreak dynamics under conditions of high exposure to contaminated water and high environmental contribution from infected individuals. These high-risk conditions intensify the transmission potential of the disease, leading to rapid spread if not properly controlled (see, Usmani et al. 2021). The graph compares two intervention strategies: one using only water treatment and the other combining water treatment with vaccination and curative treatment.

In the case of the susceptible population, the dashed green line representing water treatment only shows a steep and continuous decline. This indicates that in the absence of vaccination, nearly all individuals eventually become infected due to the elevated risk of exposure. On the other hand, the solid green line, which represents the full control strategy, demonstrates a more moderate decline in susceptibility. This is because vaccination effectively removes individuals from the pool of those at risk, slowing down the infection process and preserving a larger proportion of the population as uninfected. The contrast is even more significant in the infected population curves. The dashed red line, which represents infections under water control only, rises sharply to a high peak and remains elevated for a longer duration. This prolonged and severe outbreak is a consequence of both the high infection rate and the constant addition of bacteria into the environment by infected individuals. In contrast, the solid red line representing the full control scenario shows a substantially lower and shorter-lived peak in infections. The combination of vaccination and treatment limits new infections and accelerates recovery, thus reducing the overall burden and duration of the outbreak. Overall, the results emphasize that in high-risk environments, water treatment alone is not enough to contain a cholera outbreak. The full control strategy significantly mitigates the impact by reducing susceptibility, shortening infectious periods, and minimizing environmental contamination. This demonstrates the importance of implementing a comprehensive approach that combines multiple interventions to effectively manage and control cholera epidemics, especially in vulnerable settings.

CONCLUSION

The results of this study unequivocally demonstrated that, when it comes to controlling and managing cholera epidemics in Gombe State, Nigeria, the combined use of water treatment, vaccination, and curative therapy is far more effective than using water treatment alone. In addition to reaffirming well-established theoretical concepts, such as the crucial role that the basic reproduction number (R_0) plays in determining outbreak persistence, the study illustrated the usefulness of a holistic control approach in a real-world setting by expanding the conventional SIR-C model to incorporate multiple intervention strategies. According to the expanded model, water treatment can only lessen environmental pollution, but it is insufficient on its own, particularly in high-risk, resource-constrained environments like Gombe State where access to sanitary facilities, clean water, and healthcare is irregular.

The models demonstrated that in addition to suppressing the peak number of infections, combining water treatment with vaccination campaigns and prompt curative treatment accelerated the reduction in active cases and the recovery of the impacted population. In order to avoid recurrent outbreaks and secondary transmission, the integrated approach more effectively reduced the

DOI: 10.64290/bimagombe.v9i2A.1140

pathogen burden in the environment. These results highlight the synergistic impact of multifaceted interventions and confirm that simultaneous deployment is preferable to sequential or isolated control measure application. Furthermore, this study highlights how crucial it is to modify epidemiological models to account for the distinct environmental, infrastructure, and demographic features of a given area. The extended SIR-C framework, in contrast to generic models, was specially modified to account for the cholera dynamics in Gombe State, including the impact of seasonal rainfall, insurgency-related displacement, and deficiencies in the state's health infrastructure. The model's prediction accuracy and relevance were greatly improved by this contextualization, which also provided useful advice for legislators and medical professionals. The model's effectiveness as a decision-support tool is further supported by the fact that it was successfully validated using actual epidemic data from Gombe State (see Table 3). It gives strategic planning a mathematical basis, allowing health authorities to model different intervention scenarios, more effectively distribute resources, and predict the results of public health initiatives. By doing this, the study adds to the increasing amount of evidence that mathematical modeling is a fundamental component of epidemic preparedness and response, especially in situations when empirical data alone might not be enough to direct prompt and efficient measures. All things considered, this study not only contributes to the theoretical knowledge of cholera dynamics but also offers practical advice for bolstering epidemic management initiatives in Gombe State and other susceptible areas.

References

Andam, E.A, Apraku, L. O., Agyeil, W. & Denteh, W. O. (2015). Modelling cholera dynamics with a control Strategy in Ghana. *British Journal of Research BJR* (2(1) 031-041.

Andrews,J.R. &Basu S.(2011).transmission dynamics and control of cholera in Haiti:An epidemic model lancet 377:1248-1255.

Ashliegh, R. T., Tien, J., Eisenberg, J. M., David, J. D., Junling, M., & David, N. F.(2011). Cholera epidemic in Haiti, 2010: Using a transmission model to explain spatial spread of disease and identify optimal control interventions. Annals of Internal Medicine, 154, 593-601.

Cappasso,V. & Paveri-Fontana, S.L.(1979). A mathematical model for the 1973 Cholera epidemic in the European Mediterrenean region, Revue depidemoligie et de Sante publique, 27: 121-132.

Cheng, Y., Wang, J., & Yang, X. (2012). On the global stability of a generalized cholera epidemiological model. Journal of Biological Dynamics, 6(2), 1088–1104.

Eustace, K. A., Osman, S., & Wainaina, M. (2018). Mathematical modelling and analysis of the dynamics of cholera. Global Journal of Pure and Applied Mathematics, 14(9), 1259–1275.

Fatima, S., Krishnarajah, I., Jaffar, M. Z. A. M., & Adam, M. B. (2014). A mathematical model for the control of cholera in Nigeria. Research Journal of Environmental and Earth Sciences, 6(6), 321–325.

Feng, Z., Xia, X., Jiao, J., & Jin, Z. (2017). A multi-intervention approach to cholera control. Mathematical Medicine and Biology, 34(1), 1-13.

DOI: 10.64290/bimagombe.v9i2A.1140

Frerichs, R. R. (2005). Deadly river: Cholera and cover-up in post-earthquake Haiti. Cornell University Press.

Gaffga, N. H., Tauxe, R. V., & Mintz, E. D. (2007). Cholera: a new homeland in Africa? American Journal of Tropical Medicine and Hygiene, 77(4), 705-713.

Hantsa, K.H. &Kahsay B.N. (2020). Analysis of cholera epidemic controlling using mathematical modeling, Vol. 2020article id 7369204 pp. 1-14.

Jin, W. & Tien, J.(2011). Global stability for Cholera epidemic models.Maths, Bioscience 232.pp 31-41.

Mohammad, A. S. and Salisu, M.G.(2012). Global stability analysis of SEIR Model with holling type II incidence function. Computational and mathematical methods in medicine volume. Article ID.826052.8 pages doi 1155/2012/826052.

Mukandivire, Z.,Liao, S.,Wang,J.,Gaff, H., Smith, D.L. &Morris, G.Jr. (2011). Estimating the reproductive numbers for the 2008-2009 cholera outbreaks in Zimbabwe Proc. National Academy of science, 108 (21), 8767-8772.

Onuorah, M. O.,Atiku, F. A. &Juuko, H. (2022). Mathematical model for prevention of cholera transmission in a variable population. J. Research in Mathematics, 9(1)1 -13.

Nkuba,N. & Stephen,E.(2015). A mathematical model for the dynamics of cholera with control measures. Applied and computational mathematics Vol.4 no.22015 pp 53-63.

Nyaberi, H. O, and Malonza, D.M. (2019). A mathematical model of cholera transmission with education campaign and treatment through quarantine. Journal of Advances in mathematics and computer science 32 (3)1-12.

Rasmussen, S. A., and Mølbak, K. (2014). Cholera: An overview of its epidemiology, risk factors, and control strategies. Infectious Disease Clinics of North America, 28(3), 713-725.

Snow, J. (1855). On the Mode of Communication of Cholera. John Churchill.

Usamani, M., Brumfield, K. D., Jamal, Y., Huq, A., Colwell, R.R., Jutia, A., (2021). A review of the environmental trigger and transmission components of prediction of cholera. J. Tropical Medicine and Infections Disease. 6 (147).

Wang, J. and Modnak, C. (2011). Modelling cholera dynamics with control. Canadian Applied Mathematics. 10(3) 255 -273.

World Health Organization, (2010).cholera facts. Web page: www.who.org.

World Health Organization (2014). Website: www.who.org.

World Health Organization.(2018). Vaccine-Preventable Diseases Surveillance Standards world health Health Organization.https://www.who.int/immunization/monitoring_surv eillance/ burden /vpd/WHO Surveillance Vaccine Preventable.

World Health Organization. (2019). Cholera. https://www.who.int/news-room /fact-sheets/ detail/ cholera

Zhang, Y., Zhang, J., & Duan, Z. (2014). Seafood and cholera outbreaks: A review of recent evidence. Foodborne Pathogens and Disease, 11(1), 1-10.